



### 1. INTRODUCTION

Natural convection is the main heat transfer mode governing performances of numerous applications such as solar collectors, thermal storage systems and cooling of electrical components. Cavities containing baffles or partitions have important implications in many branches of engineering particularly in microelectronics fabrication industry, especially for the cooling of components attached to printed circuit boards, which are placed vertically. Fluids used in thermal applications such as water and mineral oils have restricted designers, because of their low thermal conductivity. Thus, nanofluids were developed to improve the heat exchange performances. Nanofluids are dilute liquid suspensions of nanoparticles with at least one critical dimension smaller than (100 nm) suspended stably and uniformly in a base liquid. The use of nanoparticles having high thermal conductivity produces a high thermal conductivity nanofluid. Many models have been proposed, focusing mainly on parameters such as geometry of nanoparticles (Hamilton (1962), Jang and Choi (2007), Chon *et al.* (2005)), Brownian effects (Houshang (2011), Nasrin and Alim (2013), Jang and Choi (2004)), temperature and interaction between nanoparticles and the base fluid (Amrollahi (2008), Chon *et al.* (2005), Li and Peterson (2006)). The first model was proposed by Maxwell (1904) showing that thermal conductivity of nanofluid increases with increasing volume fraction of solid nanoparticles. Various research works have been related with the natural convection in enclosure filled with nanofluids. Heat transfer enhancement in a two-dimensional enclosure utilizing nanofluids was investigated numerically by Khanafer *et al.* (2003). The results illustrate that the nanofluid heat transfer rate increases with an increase in the nanoparticles volume fraction. The presence of nanoparticles in the fluid is found to alter the structure of the fluid flow. These main findings are obtained in various other configurations considered by: Oztop and Abu-Nada (2008), Mahmoudi *et al.* ((2010), (2011)), Mahmoudi (2011), Mahmoudi and Sebdan (2012), Nasrin, and Alim (2013) and Hassan (2014). Kolsi *et al.* (2014) investigated numerically natural convection and entropy generation inside a three-dimensional cubical enclosure filled with water-Al<sub>2</sub>O<sub>3</sub>nanofluid. The second law of thermodynamics was applied to predict entropy generation rate. The results explain that the average Nusselt number increases when the solid volume fraction of nanoparticles and the Rayleigh number increase. Cho (2014) performed a numerical investigation into the natural convection heat transfer performance and entropy generation in a partially-heated wavy-wall square cavity filled with Al<sub>2</sub>O<sub>3</sub>-water nanofluid. For a given Rayleigh number, the mean Nusselt number increases and the total entropy generation reduces as the volume fraction of nanoparticles increases. For a given volume fraction of nanoparticles, the mean Nusselt number and total entropy generation both increase as the Rayleigh number increases. The Bejan number (ratio of heat transfer irreversibility to the

total irreversibility) reduces as the Rayleigh number increases, but is insensitive to the volume fraction of Nanoparticles. Parvin and Chamkha (2014) studied the laminar natural convection and entropy generation in a nanofluid filled complex cavity with a horizontal and a vertical portion. The cavity is filled with either water or Cu–water nanofluid. The effects on fluid flow, heat transfer and entropy generation at various Rayleigh numbers and solid volume fractions are investigated. The results show that using the nanofluid, generally leads to lowering the flow strength whereas increases the Nusselt number, entropy generation and the Bejan number. By increasing the Rayleigh number, the Nusselt number and Bejan number increase. The purpose of this work is to numerically investigate the nanofluid free convection heat transfer in a square cavity equipped by a conductive baffle. The effects of the Rayleigh number, conductivity ratio and volume fraction of nanoparticles on the flow, heat transfer and entropy generation have been examined.

### 2. MATHEMATICAL FORMULATION

Figure 1 shows a schematic diagram of the enclosure. The fluid in the enclosure is a water based nanofluid containing Al<sub>2</sub>O<sub>3</sub> nanoparticles. The nanofluid is assumed incompressible and laminar. It is assumed that the water and the nanoparticles are in thermal equilibrium. The thermo-physical properties of the nanofluid are presented in Table 1.

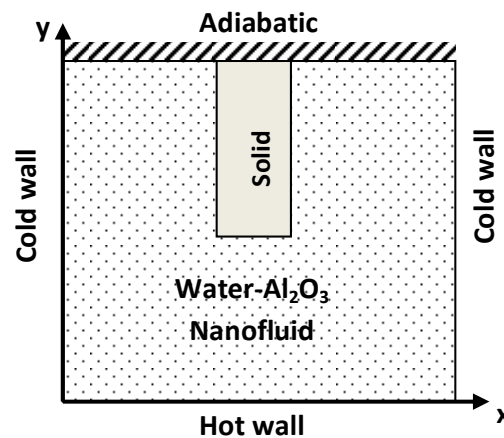


Fig.1. Problem geometry and coordinates.

Table 1 Thermophysical properties of water and Al<sub>2</sub>O<sub>3</sub> nanoparticle

Physical properties	Water	Al <sub>2</sub> O <sub>3</sub>
$C_p$ (J/kg.K)	4179	765
$\rho$ (kg/m <sup>3</sup> )	997.1	3970
$k$ (W/m.K)	0.613	40
$\alpha \times 10^7$ (m <sup>2</sup> /s)	1.47	131.7
$\beta \times 10^{-5}$ (1/K)	21	0.85

The bottom wall is maintained at a constant temperature ( $T_h$ ) higher than the right and left walls

( $T_c$ ) and the top wall is adiabatic. The thermo-physical properties of the nanofluid are assumed to be constant except for the density variation in the buoyancy term, which is approximated by the Boussinesq model.

The stream function-vorticity formulation is used to express the governing equations for the laminar and unsteady state natural convection:

Vorticity

$$\left(\frac{\partial \omega'}{\partial t'} + u' \frac{\partial \omega'}{\partial x'} + v' \frac{\partial \omega'}{\partial y'}\right) = \frac{\mu_{nf}}{\rho_{nf}} \left(\frac{\partial^2 \omega'}{\partial x'^2} + \frac{\partial^2 \omega'}{\partial y'^2}\right) + \frac{g(\phi \rho_s \beta_s + (1-\phi) \rho_f \beta_f)}{\rho_{nf}} \frac{\partial T'}{\partial x'} \quad (1)$$

Energy

$$\left(\frac{\partial T'}{\partial t'} + u' \frac{\partial T'}{\partial x'} + v' \frac{\partial T'}{\partial y'}\right) = \alpha_{nf} \left(\frac{\partial^2 T'}{\partial x'^2} + \frac{\partial^2 T'}{\partial y'^2}\right)$$

for the fluid zone (2)

$$\left(\frac{\partial T'}{\partial t'}\right) = \frac{\alpha_s}{\alpha_{nf}} \left(\frac{\partial^2 T'}{\partial x'^2} + \frac{\partial^2 T'}{\partial y'^2}\right) \text{ for the solid zone (2)}$$

Kinematics

$$\omega' = -\left(\frac{\partial^2 \Psi'}{\partial x'^2} + \frac{\partial^2 \Psi'}{\partial y'^2}\right); \alpha_{nf} = \frac{k_{nf}}{(\rho c_p)_{nf}} \quad (3)$$

The effective density of the nanofluid is given as:

$$\rho_{nf} = (1-\phi)\rho_f + \phi\rho_s \quad (4)$$

The heat capacitance of the nanofluid is expressed as (Abu-Nadu, (2008); Khanafer *et al.* (2003)):

$$(\rho c_p)_{nf} = (1-\phi)(\rho c_p)_f + \phi(\rho c_p)_s \quad (5)$$

The effective thermal conductivity of the nanofluid is approximated by the Maxwell–Garnetts model:

$$\frac{k_{nf}}{k_f} = \frac{k_s + 2k_f - 2\phi(k_f - k_s)}{k_s + 2k_f + \phi(k_f - k_s)} \quad (6)$$

The viscosity of the nanofluid is approximated as (Brinkman 1952):

$$\mu_{nf} = \frac{\mu_f}{(1-\phi)^{2.5}} \quad (7)$$

Scaling length, velocity and time by  $W$ ,  $\alpha/W$  and  $W^2/\alpha$ , and defining dimensionless temperature as  $T = (T' - T'_c)/(T'_h - T'_c)$ , the governing equations in dimensionless stream function-vorticity form are:

Vorticity

$$\left(\frac{\partial \omega}{\partial t} + u \frac{\partial \omega}{\partial x} + v \frac{\partial \omega}{\partial y}\right) =$$

$$\frac{\text{Pr}}{(1-\phi)^{0.25} \left((1-\phi) + \phi \frac{\rho_s}{\rho_f}\right)} \left(\frac{\partial^2 \omega}{\partial x^2} + \frac{\partial^2 \omega}{\partial y^2}\right) + Ra \text{Pr} \left[ \frac{1}{\frac{(1-\phi)\rho_f}{\phi\rho_s} + 1} \frac{\beta_s}{\beta_f} + \frac{1}{\frac{\phi\rho_f}{(1-\phi)\rho_s} + 1} \right] \frac{\partial T}{\partial x} \quad (8)$$

Energy

$$\left(\frac{\partial T}{\partial t} + u \frac{\partial T}{\partial x} + v \frac{\partial T}{\partial y}\right) = \left[ \frac{\frac{k_{nf}}{k_f}}{(1-\phi) + \phi \frac{(\rho c_p)_s}{(\rho c_p)_f}} \right] \left(\frac{\partial^2 T}{\partial x^2} + \frac{\partial^2 T}{\partial y^2}\right) \text{ for the fluid zone (9)}$$

$$\left(\frac{\partial T}{\partial t}\right) = R_c \left(\frac{\partial^2 T}{\partial x^2} + \frac{\partial^2 T}{\partial y^2}\right)$$

for the solid zone (9') Kinematics

$$\omega = -\left(\frac{\partial^2 \Psi}{\partial x^2} + \frac{\partial^2 \Psi}{\partial y^2}\right) \quad (10)$$

The foregoing dimensionless parameters are given as follows:

$$\text{Pr} = \frac{\nu_f}{\alpha_f} \text{ and } Ra = \frac{g \cdot \beta_f \cdot \Delta T \cdot W^3}{\nu_f \cdot \alpha_f}$$

The energy equation (conduction) needs to be solved in the solid portion of the domain. The baffle conductivity  $k_s$ , is assumed constant.

At the solid-fluid interface the temperature and heat flux must be continuous. The latter requirement is mathematically expressed as:

$$\left(\frac{\partial T}{\partial n}\right)_{nf} = R_c \left(\frac{\partial T}{\partial n}\right)_s \quad (11)$$

where  $R_c = k_s/k_{nf}$  is the thermal conductivity ratio between the material of the baffle and the nanofluid.

The associated initial and boundary conditions for the problem considered are:

For  $t \leq 0$ :

- $\omega = \Psi = \frac{\partial \Psi}{\partial x} = \frac{\partial \Psi}{\partial y} = T = 0$  (everywhere)

For  $t > 0$ :

- On the vertical left and right walls:  $\Psi = \frac{\partial \Psi}{\partial x} = T = 0$

- On the horizontal bottom wall:  $\Psi = \frac{\partial \Psi}{\partial y} = 0$ ;

$$T = 1$$

- On the horizontal top wall:  

$$\Psi = \frac{\partial \Psi}{\partial x} = \frac{\partial \Psi}{\partial y} = \frac{\partial T}{\partial y} = 0;$$

The generated entropy is written in the following form:

$$S'_{gen} = \left\{ \frac{k_{nf}}{T_0^2} \left[ \left( \frac{\partial T'}{\partial x'} \right)^2 + \left( \frac{\partial T'}{\partial y'} \right)^2 \right] \right\} + \frac{\mu_{nf}}{T_0} \left\{ 2 \left[ \left( \frac{\partial V'_x}{\partial x'} \right)^2 + \left( \frac{\partial V'_y}{\partial y'} \right)^2 \right] + \left( \frac{\partial V'_y}{\partial x'} + \frac{\partial V'_x}{\partial y'} \right)^2 \right\} \quad (12)$$

The dimensionless local generated entropy is written in the following way:

$$N_s = \frac{k_{nf}}{k_f} \left[ \left( \frac{\partial T}{\partial x} \right)^2 + \left( \frac{\partial T}{\partial y} \right)^2 \right] + \phi_s \frac{\mu_{nf}}{\mu_f} \left\{ 2 \left[ \left( \frac{\partial V_x}{\partial x} \right)^2 + \left( \frac{\partial V_y}{\partial y} \right)^2 \right] + \left[ \left( \frac{\partial V_y}{\partial x} + \frac{\partial V_x}{\partial y} \right)^2 \right] \right\} \quad (13)$$

With  $\phi_s = \left( \frac{\alpha}{W \Delta T} \right)^2 T_0$  is the irreversibility coefficient.

The first term of  $N_s$  represents the local irreversibility due to the temperatures gradients, it is noted  $N_{s-th}$ . The second term represents the contribution of the viscous effects in the irreversibility it is noted  $N_{s-fr}$ .  $N_s$  give a good idea on the profile and the distribution of the generated local dimensionless entropy. The total dimensionless generated entropy is written:

$$S_{tot} = \int_v N_s dv = \int_v (N_{s-th} + N_{s-fr}) dv = S_{th} + S_{fr} \quad (14)$$

Bejan number (Be) is the ratio of heat transfer irreversibility to the total irreversibility due to heat transfer and fluid friction:

$$Be = \frac{S_{th}}{S_{th} + S_{fr}} \quad (15)$$

Local Nusselt is given as follows:

$$Nu = \left( \frac{k_{nf}}{k_f} \right) \frac{\partial T}{\partial y} \Big|_{y=0} \quad (16)$$

The average values of Nusselt number, on the hot wall is expressed by:

$$Num = \int_0^w Nu dx \quad (17)$$

### 3. NUMERICAL METHOD

The governing Eqs. (8)–(10) were discretized using

the control-volume-finite-difference described by Patankar (1980). The central difference scheme for treating convective terms and the fully implicit procedure to discretize the temporal derivatives are retained. The grid is uniform in both directions with additional nodes on boundaries (Borjini *et al.* 2005). The resulting nonlinear algebraic equations are solved using the successive relaxation-iterating scheme (1984). The equation of radiative transfer is solved by repeatedly sweeping. The governing equations are represented by a general differential equation as follows:

$$\delta_\chi \frac{\partial \chi}{\partial t} + \frac{\partial}{\partial x} \left[ u \chi - \Gamma_\chi \frac{\partial \chi}{\partial x} \right] + \frac{\partial}{\partial y} \left[ v \chi - \Gamma_\chi \frac{\partial \chi}{\partial y} \right] = S_\chi \quad (18)$$

Where  $\chi$  stands for either  $\omega$  or  $T$  with:

$$\delta_\omega = 1, \Gamma_\omega = \frac{Pr}{(1-\phi)^{0.25} \left( (1-\phi) + \phi \frac{\rho_s}{\rho_f} \right)},$$

$$S_\omega = Ra Pr \left[ \frac{1}{\frac{(1-\phi) \rho_f}{\phi \rho_s} + 1} \frac{\beta_s}{\beta_f} + \frac{1}{\frac{\phi \rho_f}{(1-\phi) \rho_s} + 1} \right] \frac{\partial T}{\partial x}$$

$$\delta_T = 1, \Gamma_T = \frac{k_{nf}}{k_f}, S_T = 0$$

$$\Gamma_T = \frac{(\rho c_p)_s}{(1-\phi) + \phi \frac{(\rho c_p)_s}{(\rho c_p)_f}}$$

### 4. CONVERGENCE GRID TESTING AND CODE VALIDATION

An extensive mesh testing procedure was conducted to guarantee a grid independent solution. Five different mesh combinations were used for the case of  $Ra = 10^5$  and  $Pr = 6.2$ . It is found that a grid size of  $121 \times 121$  ensures an extremely grid independent solution. A time step of  $10^{-4}$  is retained to carry out all numerical tests and all results are presented for a dimensionless time equal to 2. The solution is considered acceptable when the following convergence criterion is satisfied for each step of time:

$$\sum_i^{1,2,3} \frac{\max |\psi_i^n - \psi_i^{n-1}|}{\max |\psi_i^n|} + \max |T_i^n - T_i^{n-1}| \leq 10^{-5} \quad (19)$$

A first validation (Fig. 2) test was made by comparing the present code results for  $Ra = 10^5$  and  $Pr = 0.70$  against the numerical simulation of Khanafer *et al.* (2003) in the case of differentially heated cavity. A second validation (Fig.3) was made by comparing the results of the present code with those of Oztop and Abu-Nada (2008) in the case of partially heated cavity filled by  $Al_2O_3$  nanofluid. It is clear that the present code is in good agreement with other work reported in literature as shown in Fig. 2 and Fig.3.

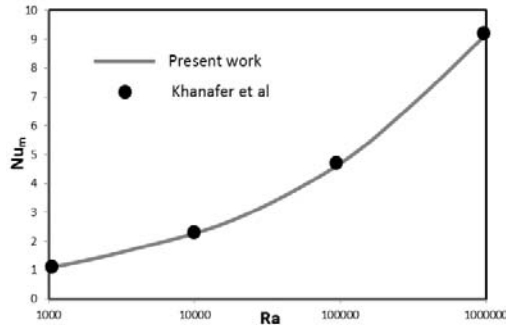


**Fig. 2. Nusselt number versus Ra number; comparison with results of Khanafer et al. (2003).**

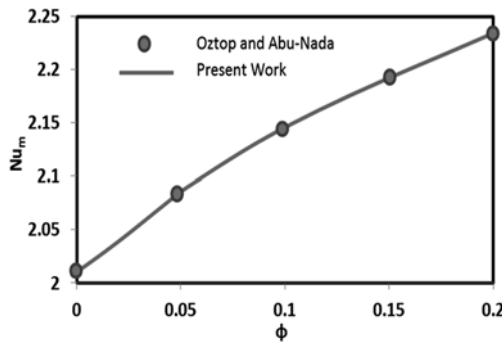


**Fig. 3. Nusselt number versus phi for Ra=10<sup>4</sup>; comparison with results of Oztop and Abu-Nada (2008).**

### 5. RESULTS AND DISCUSSIONS

The thermal fields and the flow pattern are presented respectively in Figs. 4 and 5, showing isotherms and streamlines for,  $\phi = 0$  and 0.2,  $R_c = 1$  and different Rayleigh Numbers. The fluid adjacent to vertical walls becomes cold and moves downward; after getting heated by the bottom hot wall, moves up due to buoyancy force, thus two convective cells forms inside the cavity. From Fig. 5, it is seen that the convective heat transfer becomes more important as the Ra increases, and the value of stream functions are increased showing stronger convective cells. At  $Ra = 10^6$ , there are sharp temperature gradients close to the vertical cold and the horizontal bottom hot walls.

Fluid rises up from middle portion of the bottom wall and flows down along the two vertical walls, forming two symmetric rolls with clockwise and anti-clockwise rotations inside the cavity. For  $Ra = 10^4$ , the magnitudes of stream functions are small signifying conduction dominant heat transfer within the cavity and increases slowly by increasing in the volume fraction of nanoparticles. The magnitude of stream functions increases by increasing in the solid volume fraction of nanofluid. This increase is more significant increasing Ra number. By increasing Ra, the flow structure changes from circular shaped cell, to oval shaped circulation cell. Isotherms for both  $\phi=0$  and 0.2 are almost overlapped, except near and in the conductive baffle. Thermal boundary layer is found to grow at the edge of the bottom corners and larger thickness of boundary layer is found at the top portion of sidewall. The

temperature contours occur symmetrically with respect to vertical centerline. It is seen that for  $\phi=0.2$ , the streamlines close to the walls get close to each other, thus stronger fluid flow occurs near the active walls and the temperature gradient increases resulting in enhanced heat transfer. Fig.6, presents the effect of the conductivity ratio on the flow structure and the thermal field for  $\phi = 0$  and different Rayleigh numbers. The comparison between obtained streamlines, reveals that  $R_c$  has relatively little influence on the flow. For  $R_c=0.1$ , isotherms redistributed in the baffle but with a discontinuity in the solid liquid interface. For  $R_c=1$  there is a continuity of isotherms in the baffle and the thermal field is similar to the case without baffle. It is observed that for higher  $R_c$ , the isotherms move out of the baffle: the baffle has a homogenous temperature, due to its high conductivity. This Temperature increases and becomes more uniform by increasing Rayleigh number. Fig. 7 illustrates the local Nusselt number vs. distance along the bottom wall, for  $Ra = 10^3$  and  $10^6$  and for  $\phi = 0$  and 0.2. This figure shows that due to symmetry in the temperature field, the heat transfer rate at the bottom wall ( $Nu_{loc}$ ) is symmetric with respect to the mid-length ( $x = 0.5$ ) for all Ra and  $\phi$ . Common to all Ra and  $\phi$ ,  $Nu_{loc}$  exhibits local minima at the center of the bottom wall and that has maxima at the corner points of the bottom wall. For low Rayleigh numbers it is found that  $Nu_{loc}$  values are almost constant within  $0.2 < x < 0.8$  due to the less intense heat lines. It is also observed that the larger values of heat transfer rate occur near the corner regimes of bottom wall. The local Nusselt numbers for bottom wall at  $\phi = 0.2$  is greater than that with  $\phi = 0$  especially at the corners.

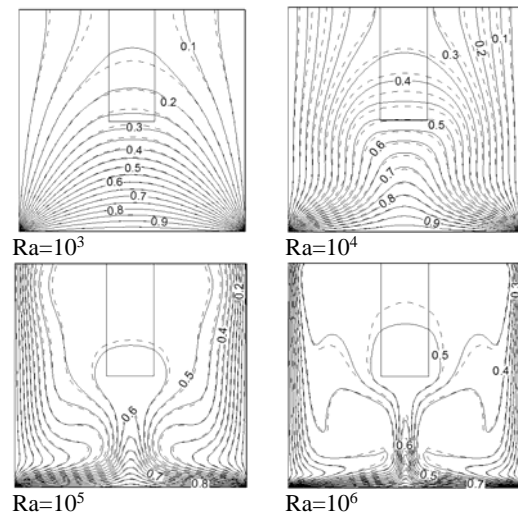


**Fig. 4. Isotherms for  $R_c=1$  and different Ra;  $\phi = 0$  (dashed);  $\phi = 0.2$  (continue).**

Figure 8, presents the variation of mean Nusselt number with volume fraction for different values of Rayleigh number. The lowest heat transfer was obtained for  $Ra=10^4$  because conduction heat transfer is the dominant mechanism of heat transfer within the cavity. The greatest heat transfer was

obtained for  $Ra=10^6$  because convection is the main mechanism of heat transfer. The figure shows also that the heat transfer increases monotonically with increasing the volume fraction for all Rayleigh numbers. Higher enhancements is obtained for  $Ra=10^6$ . In fact the enhancement in the Nusselt number when the volume fraction of nanoparticles is increased from 0 to 0.2, using  $Ra=10^6$ , is approximately 76.2% whereas the enhancement is around 71.1% for  $Ra = 10^3$ . As the Rayleigh number increases, the convection mechanism is enhanced, and thus the fluid in the cavity is perturbed more strongly, so the mean Nusselt number increases. The addition of nanoparticles increases the thermal conductivity of the working fluid, and therefore enhances the transport of the heat energy. Consequently, for all values of the Rayleigh number, the mean Nusselt number increases with an increasing nanoparticle volume fraction.

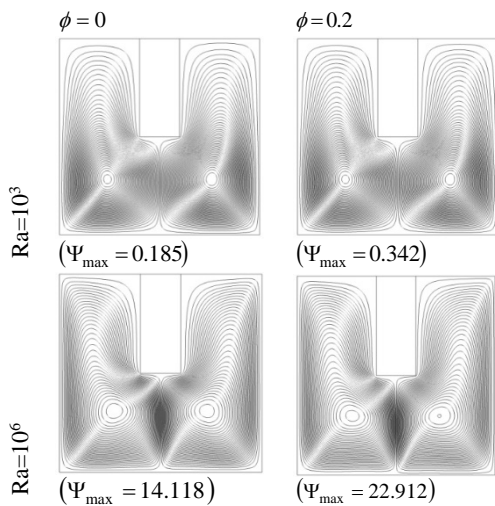


Fig. 5. Streamlines for  $Rc=1$  and different  $Ra$ .

The effect of the conductivity ratio on the average Nusselt number is presented in Fig. 9 for  $Ra=10^3, 10^4, 10^5$  and  $10^6$ . The results presented in this figure show that the increase of  $Rc$  enhance the heat transfer for all Rayleigh numbers except  $Ra=10^4$ . This behavior can be due to the transition from the conduction dominated regime to the convection dominated regime. Quantitatively, the effect of  $Rc$  is more significant for low Rayleigh numbers. In fact, when  $Rc$  is increased from 0.01 to 100,  $Nu_{av}$ , increase by about 1.15% for  $Ra=10^3$  and 0.015% for  $Ra=10^6$ .

In Fig. 10, entropy generation due to heat transfer, entropy generation due to viscous effects and total entropy are shown graphically for  $Rc=1, \phi=0.05, \phi=10^{-3}$  and different  $Ra$ . It is clear that entropy generation due to heat transfer ( $S_{th}$ ) is higher at high temperature gradients and it is concentrated at the right and left corners of the lower hot wall.  $S_{th}$  becomes more and more intense by increasing  $Ra$ . For all Rayleigh numbers distribution of local entropy generation due fluid flow covers almost whole domain except near of the top wall due to the presence of the baffle which opposes the flow and

reduce the fluid-fluid viscous effects. The covered part of the domain reduces as the Rayleigh number increases and iso-lines become more concentrated near the right and left cold walls. At  $Ra = 10^3$  and  $10^4$ , the entropy generation due to heat transfer is more influential on the contour of total entropy. For  $Ra=10^5$  it becomes a combination of entropies due to fluid friction and heat transfer. However, at  $Ra=10^6$ , the pattern of the entropy is designed by the irreversibility due to fluid friction as their values are hugely greater than the heat transfer one. Hence, it is observable that the contours of total entropy are similar to the local entropy generation due to fluid flow. Fig. 11, shows the variation of the entropy generation due to heat transfer, entropy generation due to friction and total entropy generation with the nanoparticle volume fraction for different Rayleigh numbers. As described above, under low Rayleigh number conditions, the flow within the cavity is not intense and heat transfer is dominated by conduction mode. Therefore, the entropy generation contributions of fluid friction irreversibility and heat transfer irreversibility are both low, and thus the total entropy generation rate is also low. However, as the Rayleigh number increases, the flow velocity within the cavity increases and a larger temperature gradient is formed near the active walls. As a result, the effects of fluid friction irreversibility and heat transfer irreversibility in prompting entropy generation both increase. Consequently, the total entropy generation rate increases rapidly by increasing  $Ra$ . It is seen that the total entropy generation reduces for height Rayleigh numbers as the volume fraction of nanoparticles increases. This result is explained by the fact that for height Rayleigh numbers there is a dominance of irreversibility due to friction which is decreasing with the volume fraction of nanoparticles. For smaller  $Ra$  the total entropy generation is quasi-constant for low Rayleigh numbers due to the equilibrium between entropies due to heat transfer and friction. In fact by increasing the volume fraction irreversibility due to heat transfer increases and irreversibility due to friction decreases.

A better understanding of the effects of Rayleigh number and volume fraction on entropies generation is obtained by studying the variation of Bejan number. In Fig. 12, it is noticed that at low Rayleigh numbers, Bejan number is near to unity showing the dominance of entropy due to heat transfer. This dominance is inverted by increasing Rayleigh number and Bejan number reduces significantly and entropy due to viscous effect becomes dominant. The results obtained show that the addition of nanoparticles increases Bejan number for all Rayleigh numbers showing the increase of thermal irreversibility by increasing the volume fraction.

Figure 13, presents the effect of conductivity ratio on the total entropy generation for different Rayleigh numbers. Note that the effect of the conductivity ratio on the entropy generation is not important. The variation of the entropy generation with  $Rc$  haven't the same behavior for all Rayleigh

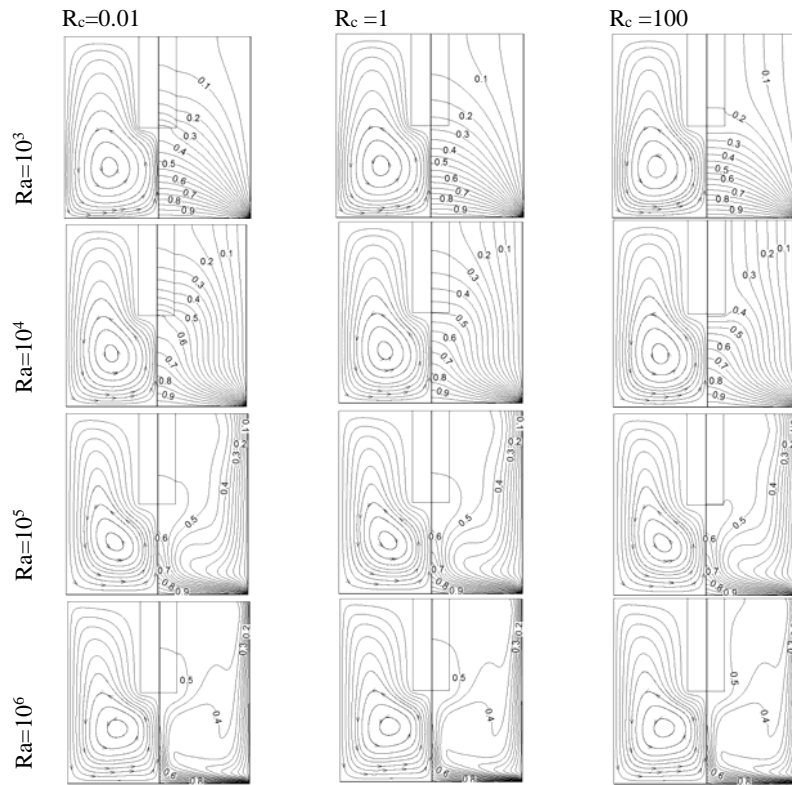


Fig. 6. Streamlines(left) and isotherms (right) for  $\phi = 0.05$ , for different Ra and different  $R_c$ .

numbers.  $S_{tot}$  is increasing for  $Ra=10^3$ , decreasing for  $Ra=10^5$  and  $10^6$  and has a minimum for  $Ra=10^4$ .

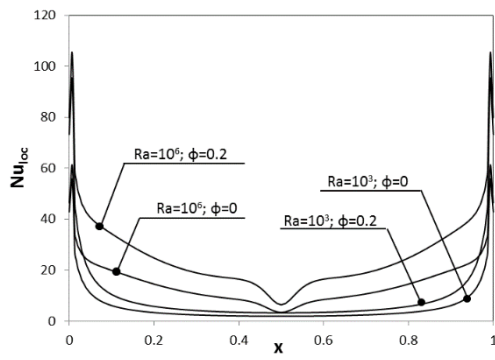


Fig. 7. Local Nusselt number at hot wall for  $R_c = 1$ .

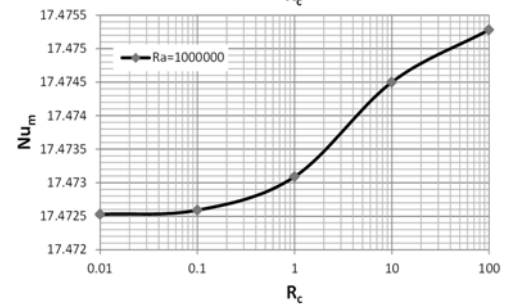
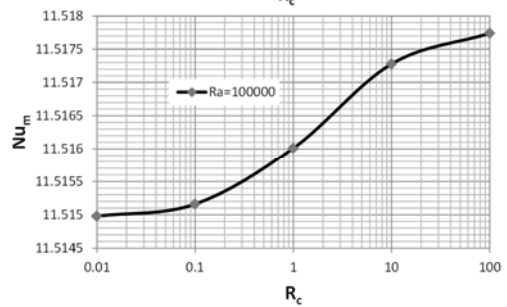
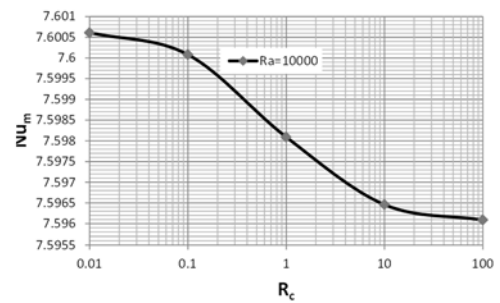
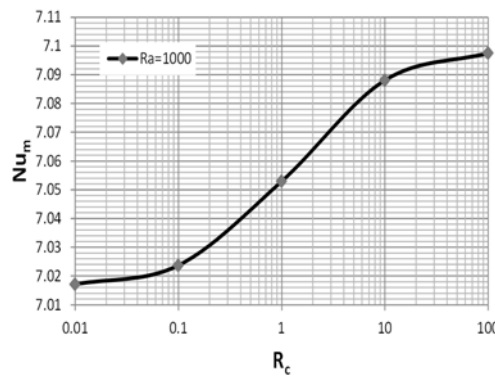


Fig. 9. Average Nusselt number versus  $R_c$  for  $\phi = 0.05$ .

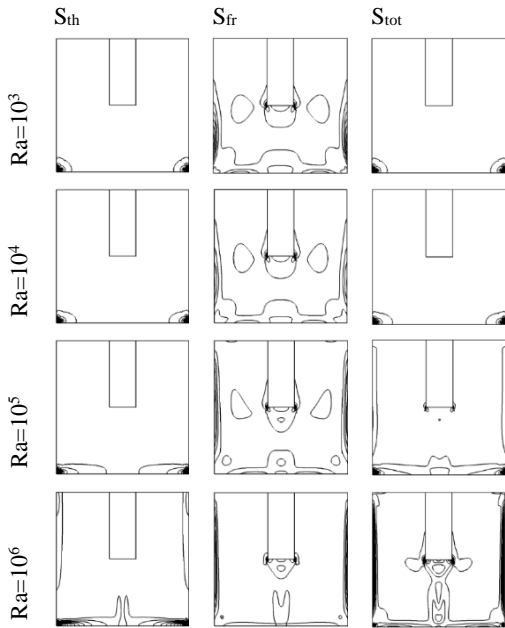


Fig. 10. Local entropies generation for  $R_c=1$ ,  $\phi=0.05$  and  $\phi=10^{-3}$ .

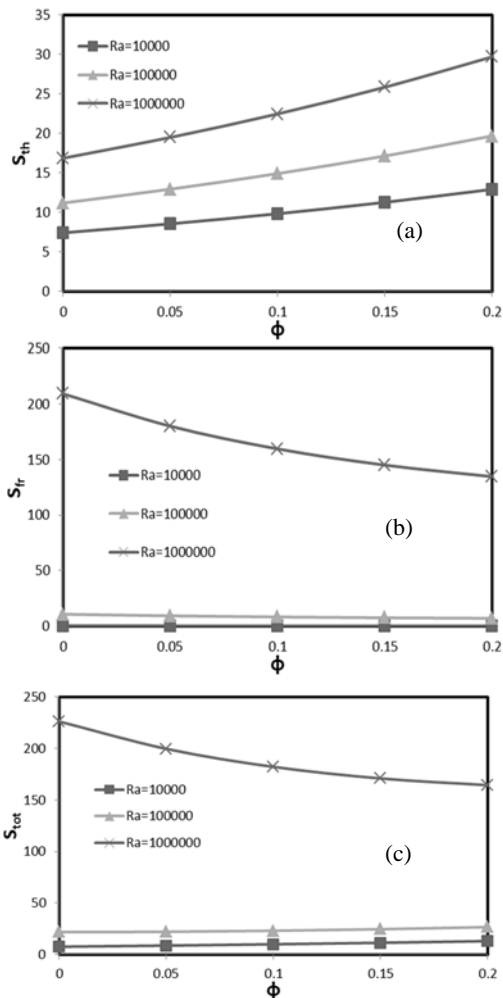


Fig. 11. Entropy generation versus  $\phi$ ; (a) Entropy due to heat transfer; (b) Entropy due to friction; (c) Total entropy.

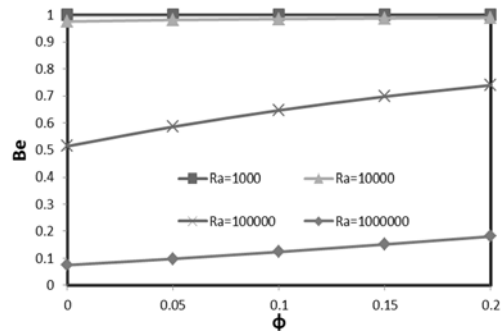


Fig.12. Bejan number versus  $\phi$ .

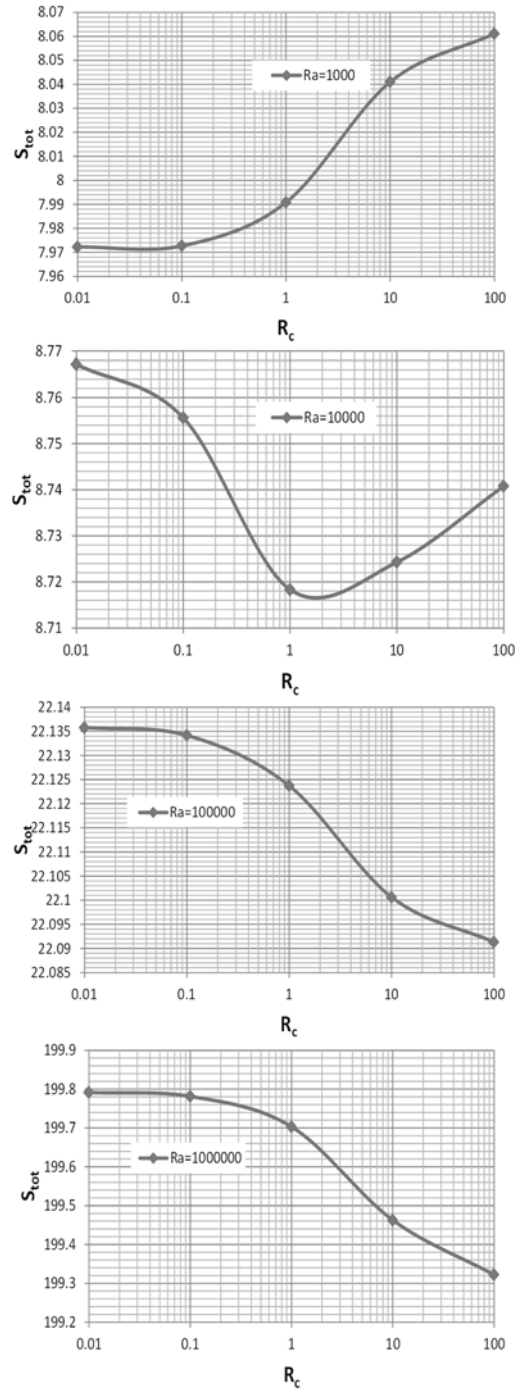


Fig. 13. Total entropy versus  $R_c$  for  $\phi=0.05$ .

## 6. CONCLUSION

This study has performed a numerical investigation into the natural convection heat transfer performance and entropy generation within an enclosure containing  $\text{Al}_2\text{O}_3$ -water nanofluid and equipped with a conductive baffle attached to the top adiabatic wall. It has been assumed that the vertical walls are cold, while the bottom wall is hot. In performing the simulations, the governing equations have been modeled using the Boussinesq approximation and then solved using the finite volume method. The simulations have focused specifically on the effects of the, nanoparticles volume fraction, the conductivity ratio and Rayleigh number on streamlines, isothermal distribution, mean Nusselt number and entropy generation within the enclosure. The results have shown that for the Rayleigh numbers considered in this study, the mean Nusselt number increases, the total entropy generation decreases and the flow strengthens with the increase of the volume fraction of nanoparticles. The effect of the conductivity ratio was found to be negligible on variations of heat transfer rate and entropy generation. Overall, the results presented in this study provide a useful insight into the natural convection heat transfer characteristics and entropy generation within enclosures containing water based nanofluids. As such, they are expected to be of benefit in optimizing heat transfer systems and minimizing energy losses for a wide range of engineering applications.

## REFERENCES

- Abu-Nada, E. (2008). Application of nanofluids for heat transfer enhancement of separated flows encountered in a backward facing step. *Int. J. Heat Fluid Flow* (29) 242–249.
- Amrollahi, A., A. A. Hamidi and A. M. Rashidi (2008). The effects of temperature, volume fraction and vibration time on the thermophysical properties of a carbon nanotube suspension (carbon nanofluid). *Nanotechnology*, (19), 315701.
- Bejan, A. (1984). *Convection Heat Transfer*. Wiley, New York.
- Borjini, M. N., L. Kolsi, N. Daous and H. Ben Aïssia (2005). Hydromagnetic double-diffusive laminar natural convection in a radiatively participating fluid. *Numerical Heat Transfer, Part A* 48, 483–506.
- Brinkman, H. C. (1952). The viscosity of concentrated suspensions and solutions. *J. Chem. Phys.* (20), 571–581.
- Ching-Chang, C. (2014). Heat transfer and entropy generation of natural convection in nanofluid-filled square cavity with partially-heated wavy surface. *International Journal of Heat and Mass Transfer* (77), 818–827.
- Chon, C. H., K. D. Kihm, S. P. Lee and S. U. S. Choi (2005). Empirical correlation finding the role of temperature and particle size for nanofluid ( $\text{Al}_2\text{O}_3$ ) thermal conductivity enhancement, *Appl. Phys. Lett.* (87), 153107.
- Hakan, F. O. and E. Abu-Nada (2008). Numerical study of natural convection in partially heated rectangular enclosures filled with nanofluids. *International Journal of Heat and Fluid Flow* (29), 1326–1336.
- Hamdy, H. (2014). Heat transfer of Cu–water nanofluid in an enclosure with a heat sink and discrete heat source. *European Journal of Mechanics B/Fluids* (45), 72–83.
- Hamilton, R. L. and O. K. Crosser (1962). Thermal conductivity of heterogeneous two-component systems. *I and EC Fundam* (1), 182–191.
- Jang, S. P. and S. U. S. Choi (2004). Role of Brownian motion in the enhanced thermal conductivity of nanofluids. *Appl. Phys. Lett.* 84, 4316–4318.
- Jang, S. P. and S. U. S. Choi (2007). Effects of various parameters on nanofluid thermal conductivity. *J. Heat Transf.* (129), 617–623.
- Khanafer, K., K. Vafai and M. Lightstone (2003). Buoyancy-driven heat transfer enhancement in a two-dimensional enclosure utilizing nanofluids. *International Journal of Heat and Mass Transfer* (46), 3639–3653.
- Kolsi, L., A. Kadhim Hussein, M. N. Borjini, H. A. Mohammed and H. Ben Aïssia (2014). Computational Analysis of Three-Dimensional Unsteady Natural Convection and Entropy Generation in a Cubical Enclosure Filled with Water- $\text{Al}_2\text{O}_3$  Nanofluid. *Arab J Sci Eng* (39), 7483–7493.
- Li, C. H. and G. P. Peterson (2006). Experimental investigation of temperature and volume fraction variations on the effective thermal conductivity of nanoparticles suspensions (nanofluids). *J. Appl. Phys.* (99), 084314.
- Mahmoodi, M. (2011). Numerical simulation of free convection of nanofluid in a square cavity with an inside heater. *International Journal of Thermal Sciences* (50), 2161–2175.
- Mahmoodi, M. and S. Mazrouei Sebdani (2012). Natural convection in a square cavity containing a nanofluid and an adiabatic square block at the center. *Superlattices and Microstructures* (52), 261–275.
- Mahmoudi, A. H., M. Shahi, A. Honarbakhsh Raouf and A. Ghasemian (2010). Numerical study of natural convection cooling of horizontal heat source mounted in a square cavity filled with nanofluid. *International Communications in Heat and Mass Transfer* (37), 1135–1141.
- Mahmoudi, A. H., M. Shahi and A. Honarbakhsh Raouf (2011). Modeling of conjugated heat transfer in a thick walled enclosure filled with nanofluid. *International Communications in Heat and Mass Transfer* (38), 119–127.

L. Kolsi/*JAFM*, Vol. 9, No. 5, pp. 2177-2186, 2016.

Maxwell, J. C. (1904). *A Treatise on Electricity and Magnetism*. Second ed., Oxford University Press, Cambridge.

Nasrin, R. and M. A. Alim (2013). Free convective flow of nanofluid having two nanoparticles inside a complicated cavity. *International Journal of Heat and Mass Transfer* (63), 191–198

Patankar, S. V. (1980). *Numerical Heat Transfer and Fluid Flow*. Hemisphere McGraw Hill, New York.

Salma, P. and A. J. Chamkha (2014). An analysis on free convection flow, heat transfer and entropy generation in an odd-shaped cavity filled with nanofluid. *International Communications in Heat and Mass Transfer* (54), 8–17